ELSEVIER

PII: S0032-3861(97)00396-0

Polymer Vol. 39 No. 5, pp. 1129–1137, 1998

0032-3861/97/$17.00+0.00

Isotherinal crystallization of isotactic polypropylene–hexamethylbenzene blends: kinetics analysis

Ali A. Alwattari and Douglas R. Lloyd*
Department of Chemical Engineering, Center for Polymer Research, The University of Texas at Austin, Austin, TX 78712, USA
(Received 6 May 1996; revised 19 April 1997)

This paper analyses the polymer crystallization kinetics (obtained via differential scanning calorimetry) for a model eutectic-forming polymer–diluent system, isotactic polypropylene (iPP)-hexamethylbenzene (HMB). The Avrami and Hoffman–Lauritzen crystallization theories were applied to iPP crystallization in the presence of HMB. In addition, an experimental–computational method of obtaining the phase diagram for an eutectic-forming system is presented along with a technique for determining the sequence of phase separation events. © 1997 Elsevier Science Ltd. All rights reserved.

(Keywords: isotactic polypropylene; kinetic analysis; Avrami analysis)

INTRODUCTION

Microporous structures of unique pore characteristics can be formed by removing thermal energy from a polymer–diluent melt-blend in which the polymer and the diluent have comparable crystallization temperatures and subsequently extracting the crystallized diluent[1]. When such an eutectic-forming polymer–diluent system undergoes crystallization, the relative kinetics of the crystallization events (and thus the order in which the components crystallize) and the polymer crystallization mechanism directly control the relative size, distribution, and morphology of the resulting pores. To control the physical structure of these microporous materials, some understanding of these kinetic and mechanistic phenomena is essential. The objective of the study reported here, as a continuation of earlier work[1,2], is to provide this understanding. This paper reports a technique for analysing the polymer crystallization kinetics obtained via differential scanning calorimetry (DSC) for an eutectic-forming polymer–diluent system over a broad polymer concentration (W_p) range.

Phase diagram generation

The crystallization rate for each component is proportional to the degree of supercooling, ΔT, for that component. To quantify ΔT (and to provide a means of representing the sequence of events) an equilibrium phase diagram is essential. This paper presents an experimental–computational method of obtaining the phase diagram for the model eutectic-forming system isotactic polypropylene (iPP) and hexamethylbenzene (HMB).

The Flory–Huggins free energy of mixing theory[3] for polymer–diluent systems[4–6] yields

$$\frac{1}{T_{m1}} - \frac{1}{T^0_{m1}} = -\frac{R}{\Delta H_1}\left[\ln \Phi_1 + \Phi_2\left(1 - \frac{r_1}{r_2}\right) + \chi r_1 \Phi_2^2\right] \quad (1)$$

* To whom correspondence should be addressed

$$\frac{1}{T_{m2}} - \frac{1}{T^0_{m2}} = -\frac{R}{\Delta H_u}\left[\frac{\ln \Phi_2}{r_2} + \Phi_1\left(1 - \frac{1}{r_2}\right) + \chi \Phi_1^2\right] \quad (2)$$

where $r_1 = V_1/V_u$ and $r_2 = V_2/V_u$ are the number of lattice units occupied by the diluent and polymer, respectively; V_1, V_2, and V_u are the molar volumes of diluent, polymer chain, and polymer repeat units[6]; Φ_i is the volume fraction of component i; and χ is the polymer–diluent interaction parameter; T_{m1} and T_{m2} are the equilibrium melting temperatures of the diluent and polymer in the mixture; T^0_{m1} and T^0_{m2} are the pure diluent and polymer equilibrium melting temperatures; ΔH_1 is the pure diluent enthalpy of fusion per mole, ΔH_u is the pure polymer enthalpy of fusion per mole of repeat units; and R is the universal gas constant.

The melting and crystallization temperatures of a symmetrical organic molecule such as HMB are known to be equal to each other and close to the equilibrium melting temperature[7]. Therefore

$$\frac{1}{T_{c1}} - \frac{1}{T^0_{c1}} \approx \frac{1}{T_{m1}} - \frac{1}{T^0_{m1}} \quad (3)$$

Substituting equation (3) into equation (1) and using experimental crystallization data, it was possible to find χ for each experimental value of Φ_1. χ was found to be independent of Φ_1.

Avrami analysis

The Avrami equation[8] is a mathematical representation of the kinetics of a single nucleation and growth process at a fixed crystallization temperature, T_c

$$1 - X = \exp(-Kt^n) \quad (4)$$

where X is the fraction of crystallizable material transformed into crystalline phase at time t; t is the time elapsed from the start of phase transformation; K is the crystallization rate constant; n is an exponent reflecting the lumped time dependence of X on the nucleation type and growth

phase dimensionality assuming constant growth rate. In a crystallizable blend, attributing X to a particular crystallizing component is a prerequisite to the application of equation (4); however, previous kinetic studies on similar systems and polymer blends had no strategy to do so[9,10].

Hoffman–Lauritzen analysis

Hoffman and Lauritzen proposed the following relation between chain-folded polymer crystal growth rate, G, the degree of supercooling, $\Delta T = T_m^0 - T_c$, and T_c[11]:

$$\ln G + \frac{U^*}{R(T_c - T_\infty)} = \ln G_0 - \frac{K_g}{T_c \Delta T f} \quad (5)$$

where:

- $K_g = 4b\sigma\sigma_e T_m^0/(\Delta H_u k)$[11]. b is iPP's chain thickness $\approx 6.26 \times 10^{-8}$ cm[12]; σ_e is the lateral surface energy ≈ 11.5 erg cm^{-2} [13,14]; ΔH_u is the pure iPP enthalpy of fusion per mole of repeat units $= 1.96 \times 10^9$ erg cm^{-3}; σ_e is the surface energy of the polymer crystal's fold surface, which is estimated from experimental data in this study.
- U^* is a constant characteristic of the activation energy for repetitive chain motion of many polymers in the molten state $= 1500$ cal mole^{-1} [11].
- R is the gas constant $= 1.987$ cal mol^{-1} K^{-1}.
- T_∞ is the theoretical temperature for the cessation of viscous flow defined as $T_\infty = T_g - 30$, [=] K, where T_g is the glass transition temperature[11], which was determined experimentally in this study.
- f is the correction factor accounting for the temperature dependence of ΔH_u; $f = 2T_c/(T_m + T_c)$.
- G_0 is the pre-exponential factor gathering quantities that are weakly dependent on temperature.
- k is the Boltzmann constant

In this study, G is approximated from experimental data and equation (5) is used to establish the effect of HMB on the iPP crystallization mechanism. The Hoffman–Lauritzen model proposes crystal growth by attachment of polymer segments perpendicular to a two-dimensional nucleus. Since these events occur on the molecular scale, details of the mechanism cannot be observed experimentally. However, a measure of the aggregate outward growth rate, G, can be measured to test the effect of independent variables in terms of the model. The growth rate of a polymer spherulite is given by:

$$G = \frac{dr}{dt} \quad (6)$$

where r is the spherulite radius. Since measurement of iPP growth was difficult under the optical microscope, crystallization rate data were obtained by differential scanning calorimetry (DSC) as outlined previously[15]. G is implicitly contained in the experimentally determined Avrami rate constant, K, generalized for any growth morphology by adopting the Avrami exponent, n[16,17]:

$$G \propto K^{1/n} \quad (7)$$

or

$$\ln G = \left(\frac{1}{n}\right) \ln K + \text{constant} \quad (8)$$

$(1/n)\ln K$ isolates changes in $\ln G$ as a function of T_c, thereby allowing a test of the Hoffman–Lauritzen equation. Therefore, K data provide relative values of iPP crystallization rate from DSC data if the value of n is known uniquely for the polymer component of the crystallizing blend. n values were determined via an Avrami analysis in this study.

MATERIALS AND METHODS

Hexamethylbenzene powder (Eastman Kodak Company, lot number D14A) and granulated iPP (iPP, Fina Oil and Chemical Co., lot number 20754, $M_w = 168\,000$; $M_n = 25\,000$) were used as received. The properties of the two components are listed in *Table 1*. The components were premixed in a borosilicate glass test tube (Borex) to give a total sample weight of 1.00 ± 0.01 g. The tube was purged with nitrogen, sealed by fusing the open end of the tube, and placed in a Tracor GCS65 convection oven for diffusive mixing at $\approx$ 500K. Samples were solidified by quenching in ice-water after 48 h. The 48 h period produced samples of uniform composition as determined by diluent extraction. The concentrations prepared were 20–100 wt% iPP at 10 wt% intervals; data are reported here for 30, 50, 70 and 90 wt% iPP. Samples containing 30, 50, 70 and 90 wt% atactic polypropylene (aPP, Himont Co., $M_w \approx 36\,000$, $M_n \approx 5000$) were prepared using the same mixing method.

ΔT was calculated as $T_m^0 - T_c$, where T_m^0 was obtained from the equilibrium phase diagram and T_c was a DSC setting, calibrated using an indium metal standard. HMB crystallization temperature in a mixture, T_{cl}, was measured by cooling homogeneous melt blends at -10K min^{-1} using a Perkin-Elmer DSC7 for iPP weight fractions $W_p = 0.10$–0.70. These concentrations exhibited a distinct diluent crystallization peak prior to the eutectic crystallization peak. For concentrations $W_p > 0.75$, the HMB crystallization peak merged with the eutectic crystallization peak, within which HMB and iPP crystallization were incorporated, and T_{cl}, was not distinguishable. Therefore, for $W_p > 0.75$, T_{cl} was determined by using aPP–HMB blends, since no crystallization peak was contributed by aPP.

The validity of incorporating aPP–HMB data rests on the assumption that the atactic PP enviromnent is thermodynamically equivalent to a supercooled iPP environment; that is, χ at a given polymer concentration is determined by liquid phase dispersive interactions, which are independent of tacticity and polymer molecular weight[23]. Equation (1) indicates the ratio r_1/r_2 determines the role of polymer molecular weight on diluent T_m depression. In this study $r_1 \approx 3$ and thus $(r_1/r_2) \ll 1$ for both iPP and aPP polymers. Therefore, the molecular weight difference in polymers should not influence the extent of diluent temperature depression by the two different polymers. Thirty, 50, 70 and 90 wt% aPP samples were prepared to experimentally confirm the equivalence of the depression effect between the two polymers. Within experimental

Table 1 Physical property values used in thermodynamic analysis of iPP-HMB. Molar volume V and density ρ refer to the molten state of the component

iPP				
V_u (ml mol^{-1})	ρ_2 (g ml^{-1})	ΔH_u (J mol^{-1})	T_{m2}^0 (K)	r_2
49.5[18]	0.85[18]	6930[19]	460.5[20]	577[b]
HMB				
V_1 (ml mol^{-1})	ρ_1 (g ml^{-1})	ΔH_1 (J mol^{-1})	T_{m1}^0 (K)	r_1
152.7[21]	1.061[a]	19760	441.0	3.08

[a] ρ_1 was estimated from V_1 and the molecular weight of HMB.
[b] r_2 was estimated as $M_n/(\rho_2 \cdot V_u)$ based on $M_n \approx 24\,300$.
ΔH_1 was obtained by DSC at -10K min^{-1} and agrees within 3% with published data[22].

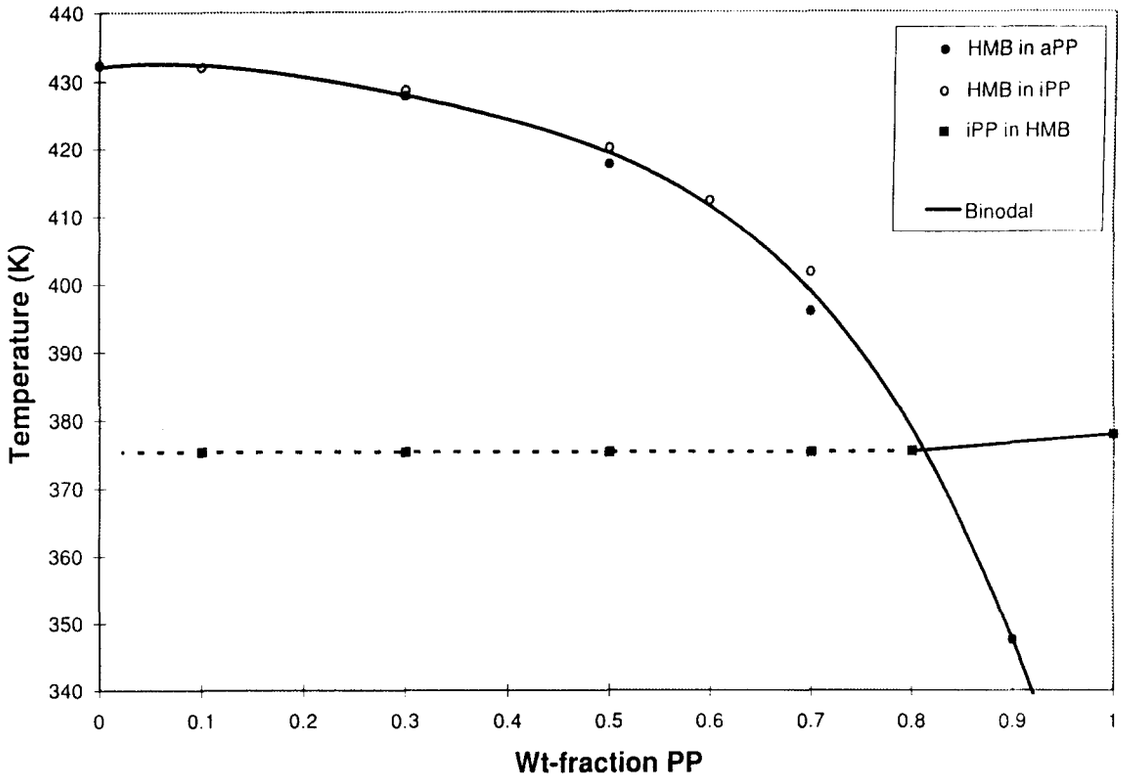

Figure 1 Dynamic phase diagram (-10K min^{-1}) for iPP–HMB and aPP–HMB

error, the crystallization temperature of the HMB was the same in both polymers, as shown in *Figure 1*.

For the isothermal kinetic analysis, polymer concentrations of 20–100 wt% crystallized at T_c ranging from 387 to 401K are reported.

RESULTS AND DISCUSSION

Phase diagrams

T_{c1} data obtained at -10K min^{-1} in the presence of iPP and aPP as well as the T_{c2} data obtained at -10K min^{-1}, are shown in *Figure 1*. The graphical match of the HMB depression curves in iPP and aPP suggests diluent crystallization temperature depression is independent of the tacticity and crystallizability of the polypropylene. The eutectic point of the phase diagram (*Figure 1*) generated at -10K min^{-1} occurs at 375.0 ± 1K and 0.75 iPP.

Equilibrium T_{m1} values were approximated by using the dynamic experimental values of $1/T_{c1} - 1/T_{c1}^0$ determined in this study (shown in *Figure 1*) along with equation (3) and a literature value of T_{m1}^0 (441.1 + 0.1K). The results are shown in the first column of data in *Table 2*. Equilibrium T_{m1} was also computed from equation (1), coupled with the same literature value of T_{m1}^0 (see the second column of data in *Table 2*). The results of these two methods of estimating T_{m1} show excellent agreement. The computed values were used to plot *Figure 2*.

Using the T_{m1} data shown in *Figure 1* with equations (1) and (3) and the data in *Table 1*, χ was estimated at each experimental polymer concentration studied. A concentration independent average χ value of 0.11 ± 0.02 was found to represent the polymer concentration range 10–90 wt%. Composition independence is in agreement with other non-polar polymer–diluent systems[6]. The estimation of χ based on diluent crystallization temperature depression data in eutectic forming systems was originally proposed by Wittmann *et al.* for the system poly(ϵ-caprolactone) and trioxane[24] and by Hodge *et al.* for the system polyethylene and 1,3,5-tri-bromobenzene[25].

χ obtained above was substituted into equation (2) and T_{m2} was computed using the pure iPP equilibrium temperature cited in *Table 1*. The results are shown in

Table 2 Experimental and computed equilibrium melting temperatures of iPP and HMB

W_p	T_{m1} (K)	T_{m1} [equation (1)] (K)	T_{m2} (experimental) (K)	T_{m2} [equation (2)] (K)
0.00	441.1 ± 0.1	441.0	—	—
0.10	440.7 ± 0.2	440.7	424 ± 9	414
0.20	439.7 ± 0.2	438.7	422 ± 9	417
0.30	437.3 ± 0.2	437.4	424 ± 8	422
0.50	426.0 ± 0.2	428.7	437 ± 5	431
0.60	—	420.3	438 ± 5	436
0.70	—	407.8	436 ± 8	442
0.90	—	354.9	447 ± 6	454
1.00	—	—	461 ± 4	461

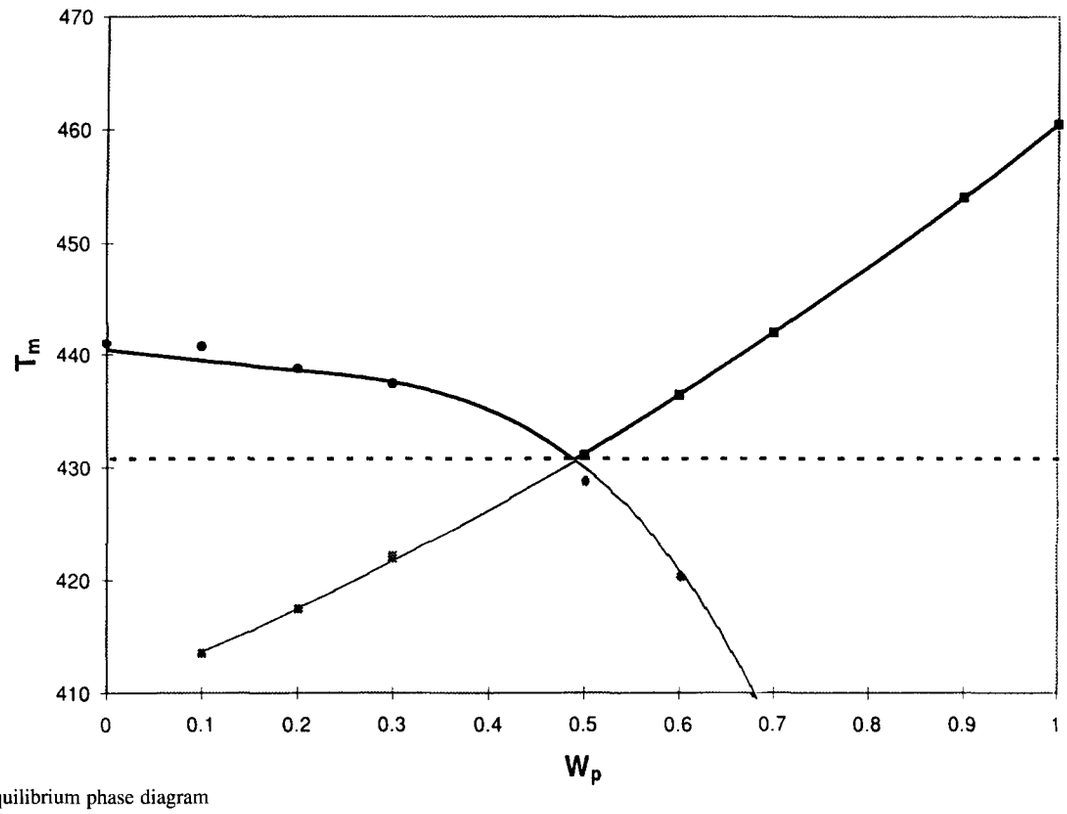

Figure 2 Equilibrium phase diagram

Table 2 along with experimental values generated using the Hoffman–Weeks method[26,27]. The confidence limits on the experimental T_{m2} are large, due to the inaccuracy of the Hofftnan–Weeks method. The confidence limits on the estimated T_{m2} were less than ± 2K based on propagating the ±0.02 uncertainty in the average χ value into equation (2).

The computed values of T_{m2} were used in the equilibrium phase diagram shown in *Figure 2*. The equilibrium eutectic coordinates, T_E and W_E, were estimated at the intersection point of equations (1) and (2), giving (T_E, W_E) = (431 ± 1 K, 0.50 ± 0.02). Using the experimental T_{m2} data yields an eutectic point of (433 ± 4K, 0.45 ± 0.05).

Sequence of phase transitions and phase identification

To determine the sequence of crystallization events, the polymer concentration of the residual melt was ascertained as a function of time during isothermal crystallization. Once the phase transition sequence and their corresponding DSC exotherm energies were identified, an Avrami analysis was performed.

Preliminary experiments indicated the isothermal crystallization temperatures at which iPP crystallization data was accessible to DSC observation were below the eutectic temperature shown in *Figure 2*. At these temperatures the crystallization of both components is thermodynamically possible. Therefore, the contribution from a particular component to the DSC energy flow (Q_t) at T_c must be established in order to proceed with quantitative analysis of the kinetic data. Phase transitions are considered to occur in three stages: (a) prior to, (b) during, and (c) after the onset of isothermal polymer crystallization.

(a) Phase transitions prior to the onset of isothermal polymer crystallization. For blends of polymer concentration less than the dynamic (-10K min^{-1}) eutectic concentration, a diluent crystallization peak preceded any polymer crystallization peak during cooling of the melt, which is in agreement with literature reports[28]. For such cases, the mass of HMB crystallized prior to the onset of polymer crystallization was estimated by dividing the area of the diluent crystallization peak by the pure HMB heat of crystallization. To determine the heat of crystallization for pure HMB, three such samples were crystallized in a DSC at -10K min^{-1} from 493 to 323K. The heat of crystallization was 122 ± 2.2 J g^{-1} or 19.7 kJ mol^{-1} with a peak temperature of 432.0 ± 0.2K, which agrees within < 3% of published data[22]. The resulting melt phase polymer concentration, L, from which iPP isothermally crystallizes, was calculated using a material balance. The results shown in *Table 3* indicate the liquid phase prior to the onset of iPP exotherm contains 73.4 ± 3.9 wt% iPP regardless of the initial iPP concentration.

To make use of this experimental (-10K min^{-1}) value of L in the equilibrium analysis, two arguments are presented. First, it is necessary to prove that no iPP crystallization occurs during step (a) of an actual isothermal experiment. To simulate step (a), a 30 wt% iPP sample was quenched using a DSC from the melt to 392K and held for

Table 3 Estimate of amorphous iPP concentration (L) prior to onset of iPP crystallization as a function of the initial iPP concentration

W_p	L (wt% iPP)	Area excess HMB per mg of sample (mJ)	Peak T_c (K)
0.10	76.8 ± 2.34	1031 ± 22.6	431.8 ± 0.2
0.20	75.5 ± 0.47	449.1 ± 0.9	430.0 ± 0.2
0.30	69.8 ± 1.70	233.7 ± 1.9	428.5 ± 0.1
0.40	69.9 ± 0.84	129.8 ± 1.0	424.7 ± 0.2
0.50	71.6 ± 0.97	72.5 ± 0.4	419.8 ± 0.1
0.60	76.2 ± 0.24	43.4 ± 0.5	412.0 ± 0.1
0.70	77.6 ± 0.12	17.1 ± 0.2	401.5 ± 0.2

Table 4 HMB crystallization area as a function of cooling rate

Weight fraction iPP	DSC cooling rate (K min^{-1})	Peak area (mJ)
0.75	30	48
0.75	10	54
0.75	2	46
0.50	30	387
0.50	10	360
0.50	2	383
0.30	30	572
0.30	10	537
0.30	2	559

Table 5 Area comparisons for checking phase identity after the onset of iPP crystallization

W_p	Sample weight (mg)	Total measured area under exotherm (mJ)	A_{MAX} (mJ)
0.20	8.25	148.7 ± 10.0	141.6 ± 7.6
0.30	8.78	244.2 ± 9.2	226.1 ± 12.1
0.40	8.58	327.5 ± 14.4	294.6 ± 15.7
0.50	10.87	514.3 ± 24.9	466.5 ± 24.9
0.60	9.24	525.2 ± 26.4	475.8 ± 25.4
0.70	10.82	741.3 ± 22.2	650.1 ± 34.7

0.2, 2.0 and 8.0 min, respectively. Upon remelting, only the 8 min experiment displayed a polymer melting peak. Therefore, no iPP crystallized at 392K until after an onset period of at least 2 min had elapsed. Similar results were obtained for other crystallization temperatures and melt blend compositions. Second, the material balance computations are assumed to be valid during the isothermal quench used to reach T_c. To support this assumption, the effect of cooling rate on the excess diluent peak area was determined at three initial iPP concentrations. The results shown in *Table 4* confirmed HMB peak area, and therefore L, can be considered to be independent of cooling rate. Consequently, it is concluded that $L = 73.4 \pm 3.9$ wt% iPP during the period prior to the onset of isothermal iPP crystallization.

(b) Phase transitions during the onset of iPP crystallization. The second peak to evolve during the dynamic crystallization represents the crystallization of both polymer and any diluent not crystallized in the diluent crystallization peak. The sequence of crystallization events within this single eutectic peak cannot be resolved by simply using DSC data at -10K min^{-1}. However, HMB in the eutectic mixture can be assumed to crystallize faster than iPP in the T_c range investigated in this study. This postulation is based on the relative crystallization kinetics of the pure components. For a macromolecule there exists a significant surface energy barrier that must be overcome upon crystallization[29]. Because of this additional energy barrier, nucleation and subsequent chain-folded polymer crystallization are only possible at a T_c considerably lower than the equilibrium melting temperature of the polymer in the blend; that is, in a supercooled state that provides negative free energy to counteract the positive surface energy. HMB is unlikely to require such large supercooling because small molecules nucleate and grow without chain-folding and grow rapidly, even at small supercoolings[30]. This mechanistic difference was demonstrated experimentally by isothermal crystallization of pure iPP and pure HMB using DSC. With a supercooling of 4K, pure HMB crystallized completely in less than 2.5 min; whereas pure iPP tended to take an infinite time to crystallize. Even at a supercooling of 62K, pure iPP required approximately 85.5 min to crystallize.

To determine the sequence of crystallization events in iPP–HMB blends during the onset of iPP crystallization, thermo-optical microscopy observation of the sequence of crystallization events in an eutectic blend was used. A film (weight $\approx$ 10 mg, thickness < 100 μm) of the -10K min^{-1} 75 wt% iPP was placed between glass cover slips (American Scientific Products) and into a Mettler FP 82 hot stage at 493K. To minimize diluent loss at high temperatures, the cover slips were sealed using a combination of thin Teflon tape wrapped on the edges of one slip plus a light coat of silicone vacuum grease on the second slip. The stage was programmed to cool at its fastest rate (-20K min^{-1}) to a crystallization temperature of 398K, a value within the temperature range at which isothermal DSC data were collected. A clear supercooled melt was observed and photomicrographed to identify the evolving structures. The thermo-optical microscope experiment indicated HMB crystal growth was complete in less than 2 min, and prior to any observable polymer crystallization. Therefore, iPP crystallization occurs after the excess and eutectic HMB have crystallized for $W_p \leq 0.75$.

(c) Phase transitions after the onset of iPP crystallization. Based on a calibration of the enthalpy of crystallization for pure iPP, the maximum area contribution (A_{MAX}) due to the iPP in a particular sample was computed. This calculation was done by multiplying the known weight of polymer in a blend sample by the pure iPP enthalpy of fusion:

$$(\text{mass iPP in sample}) \times (\Delta H_{iPP}) = A_{MAX}$$

A_{MAX} was compared to the experimental isothermal exotherm areas collected at different T_c and polymer concentrations. If the two numbers did not differ by a statistically significant amount, then part (c) of the exotherm was considered to be pure iPP. Typical results, as shown in *Table 5*, indicate that within experimental error the exotherm areas in the T_c range investigated were fully accounted for by iPP.

For samples containing more than 75 wt% iPP, the relative contributions of the two components could not be isolated by the above method. Therefore, a different analysis and interpretation of kinetic data was required, as discussed below.

Avrami analysis

The Perkin-Elmer Series 7 DSC software provided values of the area (Q_t) between time zero and a subsequent time t, and the total exotherm area, Q_0. The fractional area (Q_t/Q_0) at time t is equivalent to the fractional phase conversion X as defined in equation (4). Plots were made of the linearized form of the Avrami equation, $\ln(-\ln(1-X))$ *versus* $\ln t$, for polymer concentrations $W_p = 0.20$, 0.40, 0.60 and 1.00. Linearity of the Avrami plots was assessed using a Statview® statistical package and resulting values for n and K are listed in *Table 6*, along with the independent variables W_p, T_c and ΔT. Plots of $\ln(-\ln(1-X))$ *versus* $\ln t$ for 80 wt% iPP (at $T_c = 387$–390K) and 90 wt% iPP (at T_c 389–393K) proved to be non-linear. The n values for the samples of $W_p < 0.60$ agreed with the n values for pure iPP, within experimental error. Experimental error is attributed to the determination of the exotherm zero time, which determines both the value of the total amount of

Table 6 K and n determined from regression fit of Avrami's model

W_p	T_c (K)	ΔT (K)	$K \times 10^3$	n
1.00	401.2	59.3	0.92 ± 0.25	2.14 ± 0.04
1.00	400.2	60.3	1.40 ± 0.36	2.11 ± 0.08
1.00	399.2	61.3	1.53 ± 0.15	2.19 ± 0.02
1.00	398.2	62.3	3.18 ± 0.70	2.16 ± 0.05
0.70	395.0	46.9	1.14 ± 0.46	2.06 ± 0.01
0.70	394.0	47.9	1.72 ± 0.31	2.11 ± 0.04
0.70	393.0	48.9	2.65 ± 0.19	2.18 ± 0.01
0.70	392.0	49.9	5.96 ± 0.88	2.15 ± 0.01
0.60	396.0	40.4	0.77 ± 0.25	2.19 ± 0.05
0.60	395.0	41.4	1.27 ± 0.11	2.21 ± 0.02
0.60	394.0	42.4	2.43 ± 0.31	2.14 ± 0.02
0.60	393.0	43.4	3.28 ± 0.38	2.14 ± 0.06
0.60	392.0	44.4	5.24 ± 0.62	2.17 ± 0.03
0.50	395.0	36.1	0.42 ± 0.06	2.28 ± 0.02
0.50	394.0	37.1	1.16 ± 0.21	2.19 ± 0.03
0.50	393.0	38.1	2.42 ± 0.44	2.17 ± 0.03
0.50	392.0	39.1	3.40 ± 0.56	2.25 ± 0.04
0.50	391.0	40.1	8.06 ± 0.82	2.24 ± 0.04
0.40	394.0	37.1	1.14 ± 0.50	2.13 ± 0.07
0.40	393.0	38.1	2.30 ± 0.35	2.11 ± 0.05
0.40	392.0	39.1	4.10 ± 0.18	2.20 ± 0.01
0.40	391.0	40.1	6.79 ± 0.03	2.22 ± 0.01
0.30	394.0	37.1	1.67 ± 0.17	2.03 ± 0.02
0.30	393.0	38.1	3.58 ± 0.22	2.08 ± 0.01
0.30	392.0	39.1	4.63 ± 1.66	2.05 ± 0.07
0.30	391.0	40.1	7.48 ± 1.32	2.22 ± 0.04
0.20	393.2	37.9	3.11 ± 0.24	2.03 ± 0.06
0.20	392.2	38.9	7.81 ± 0.84	1.97 ± 0.05
0.20	391.2	39.9	14.18 ± 0.65	2.01 ± 0.03
0.20	390.2	40.9	16.96 ± 1.59	2.17 ± 0.05

crystallization energy, Q_0, and the abscissa of the Avrami plot, $\ln t$. The precision of the zero time is determined by the error associated with the extrapolation of the baseline (typically 1–2%.). Via propagation of errors techniques, it has been proposed[31,32] that a mere 1% zero time error can cause non-integral value deviations of n, despite a good line fit.

As mentioned above, material balances prior to and during the onset of iPP crystallization suggest iPP crystallization is the dominant contributor to Q for $W_p < 0.75$. Therefore, it is not surprising that the n values for these polymer concentrations are similar to pure iPP in the temperature range investigated. This agreement also indicates the crystallization of the HMB prior to any significant iPP crystallization did not prevent iPP from conforming to the Avrami equation.

Effect of δT on (1/n) lnk and n

$(1/n)\ \ln K$, as a measure of polymer crystallization rate, is plotted *versus* ΔT in *Figure 3* for polymer concentrations < 75 wt% iPP; representative error bars are shown for the 30 wt% sample. $(1/n)\ \ln K$ is seen to increase as ΔT was increased, but within experimental error remains independent of polymer concentration, which is reasonable since polymer crystallization occurred from a fixed liquid phase polymer concentration, L, as shown above.

Table 6 indicates $n \approx 2$ for the pure iPP samples, which is in agreement with literature data in the same T_c range[33,34]. *Table 6* also indicates $n \approx 2$ for all other samples, which implies instantaneous nucleation coupled with a truncated sphere or other two dimensional morphology[29]. The concept of premature growth termination by impingements and a value of $n = 2$ is supported by the physical model of the growth process. This model[35] proposes that the incremental growth process prior to the spherulite is a two-dimensional lamella leading to $n = 2$ in Wunderlich's scheme. Stein and Powers[36] and Escleine *et al.*[37] derived that truncation by sample thickness results in a reduction of the Avrami exponent when compared to n obtained from bulk samples via dilatometry. For a sample that is a few hundred

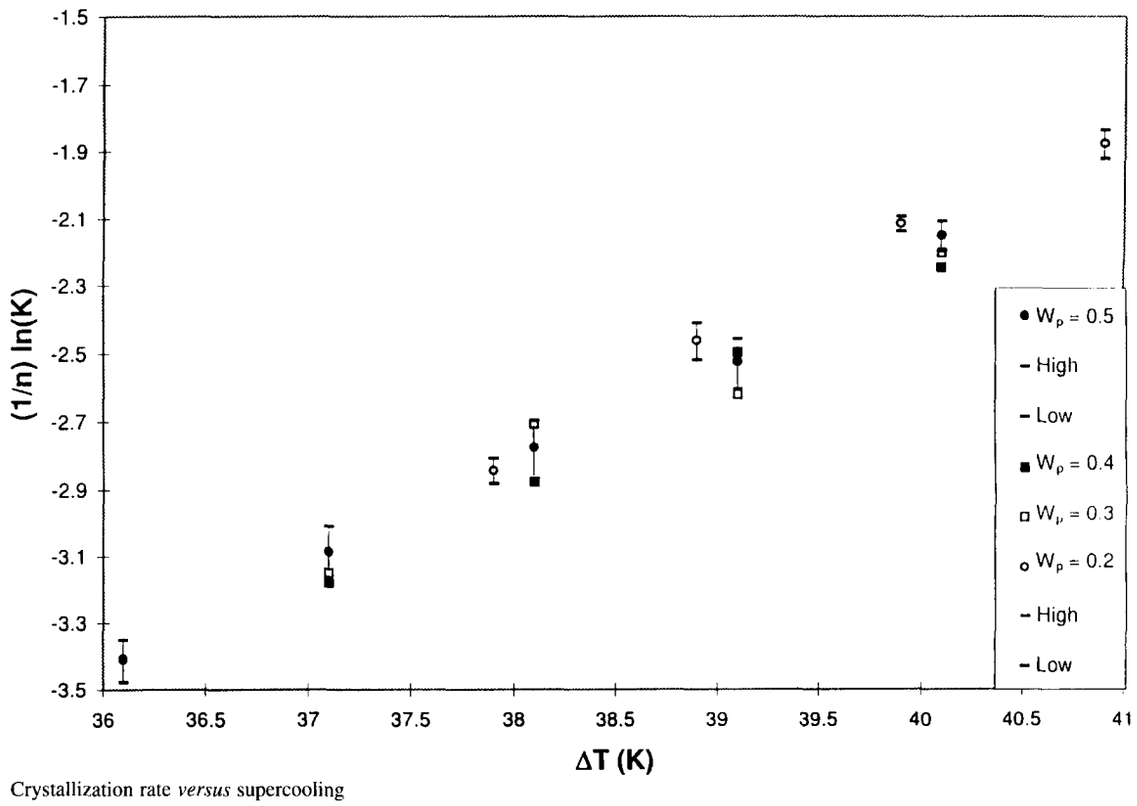

Figure 3 Crystallization rate *versus* supercooling

micrometers thick, as samples in this study were, the boundaries of the sample represent truncation of the volume out of which a full spherulite could emerge. The greater the ratio of spherulite diameter to sample dimensions, the greater the truncated fraction. Scanning electron microscopy and transmission electron microscopy confirms this lamellar and spherulitic structure for the isothermally crystallized samples[2]. In the case of the HMB diluted samples, iPP spherulite deformation was caused by impingement with adjacent HMB crystals. The Stein and Powers concept of truncation can be extended to this case because HMB crystals represent a volume from which spherulite expansion is truncated. This truncation is analogous to truncation at sample boundaries. Therefore, a contribution to $n = 2$ may exist from diluent truncation of spheruhtes, mutually impinging spherulites, and sample thickness constraints since all these factors tend to cause two-dimensional growth.

Crystallization kinetics for $W_p > 0.75$

As indicated above, Avrami plots for 80 and 90 wt% iPP proved to be non-linear. Consider an 80 wt% iPP sample supercooled to $T_c = 383$K. According to the extrapolated phase diagram (*Figure 2*), if the supercooled liquid polymer concentration remains at 80 wt% iPP during the quench, diluent crystallization is not possible since T_c is greater than the crystallization temperature of the supercooled HMB. The existence of a supercooled melt initially fixed at 80 wt% iPP is reasonable since the polymer concentration and viscosity are high and HMB crystallization is impeded by diffusional limitations[1,38]. Under these conditions, the onset of iPP crystallization should precede HMB crystallization, and HMB crystallization is prevented until enough iPP crystallizes for the supercooled liquid polymer concentration to move to the left of the extrapolated diluent phase boundary. At this polymer concentration, a driving force exists for the of remaining components to crystallize. Thus, the curvature in the Avrami plot is most likely a result of polymer crystallization followed by simultaneous crystallization of remaining polymer plus diluent; that is, two separate crystallization steps occurred. The proposed sequence of crystallization events was substantiated by SEM photomicrographs that showed needle-like pores resident at the boundaries of dense spherulites (*Figure 4*), indicating iPP spherulitic growth preceded diluent crystallization. Had HMB crystallized first, a random distribution of pores would have been observed, around which iPP spherulites would appear[1]. Experimentally, the 80 and 90 wt% iPP samples demonstrated asymmetry in their DSC exotherms and double melting peaks.

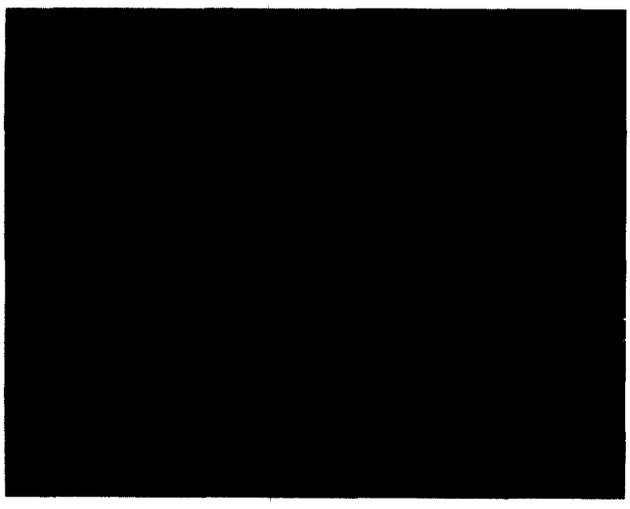

Figure 4 Scanning electron micrograph showing voids left upon removal of crystallized HMB at the boundary of iPP spherulites

Hoffman–Lauritzen analysis

Figure 5 show regression fits to test equation (5), wherein the quantity $[(1/n)\ln K + U^*/(R(T_c - T_g - 30)]$ was plotted *versus* the independent variable grouping $T_m/T_c(\Delta T)f$. The slope of a straight line through the data is equal to the quantity $4b\sigma\sigma_e/\Delta H_u k$[39–41]. Based on residual analysis, the departures of individual data points from the lines were not significantly greater than the experimental reproducibility of $(1/n)\ln K$. Therefore, the model predicts the data reasonably well, showing a strong negative temperature coefficient and the chain-folding mechanism known to govern the crystallization of pure iPP persist in the eutectic forming system. The fold surface energy of iPP crystals was estimated from the slope $4b\sigma\sigma_e/\Delta H_u k$ and used below.

Effect of the independent variables T_c and W_p on iPP crystallization kinetics

An explicit equation for T_m of iPP in Kelvin as a function of polymer concentration was obtained by fitting the polymer phase boundary in *Figure 2* to a linear equation:

$$T_m = 431 \pm 1 + 59(W_p - 0.5) \text{ for } W_p > 0.50 \quad (9)$$

$$T_m = 431 \pm 1 \text{ for } W_p < 0.50 \quad (10)$$

Coupling these functions with equations (5)–(8), the Hoffmen–Lauritzen test results can be summarized by the following two equations:

for $W_p > 0.50$,

$$\frac{1}{n}\ln K + \frac{U^*}{R(T_c - T_g + 30)} = C_1 - \left(\frac{4b\sigma\sigma_e}{\Delta H_u k}\right)\frac{431 + 59(W_p - 0.5)}{T_c f(431 + 59(W_p - 0.5) - T_c)} \quad (11)$$

where C_1 is a temperature independent constant for a given polymer concentration greater than 50 wt% iPP.

for $W_p < 0.50$,

$$\frac{1}{n}\ln K + \frac{U^*}{R(T_c - T_g + 30)} = C_2 - \left(\frac{4b\sigma\sigma_e}{\Delta H_u k}\right)\frac{431}{T_c f(431 - T_c)} \quad (12)$$

where C_2 is a temperature independent constant for a given polymer concentration less than 50 wt% iPP.

Equations (11) and (12) were used to investigate the effect of W_p on crystallization rate for a given driving force ΔT. Note, at a fixed ΔT there should be no significant differences in the heterogeneous nucleation density[42,43], allowing isolation of the effect of W_p on $(1/n)\ln K$ at the same thermodynamic driving force. A supercooling at which data were available for most polymer concentrations was selected ($\Delta T = 39$K). $(1/n)\ln K$ had to be estimated using equation (11) for polymer concentrations 70 and 100 wt% iPP. The results are shown in *Table 7*. The value of K^n for pure iPP is in agreement with literature data for iPP[44].

From *Table 7*, at a fixed ΔT and $W_p < 0.50$, iPP is estimated to crystallize four orders of magnitude faster than

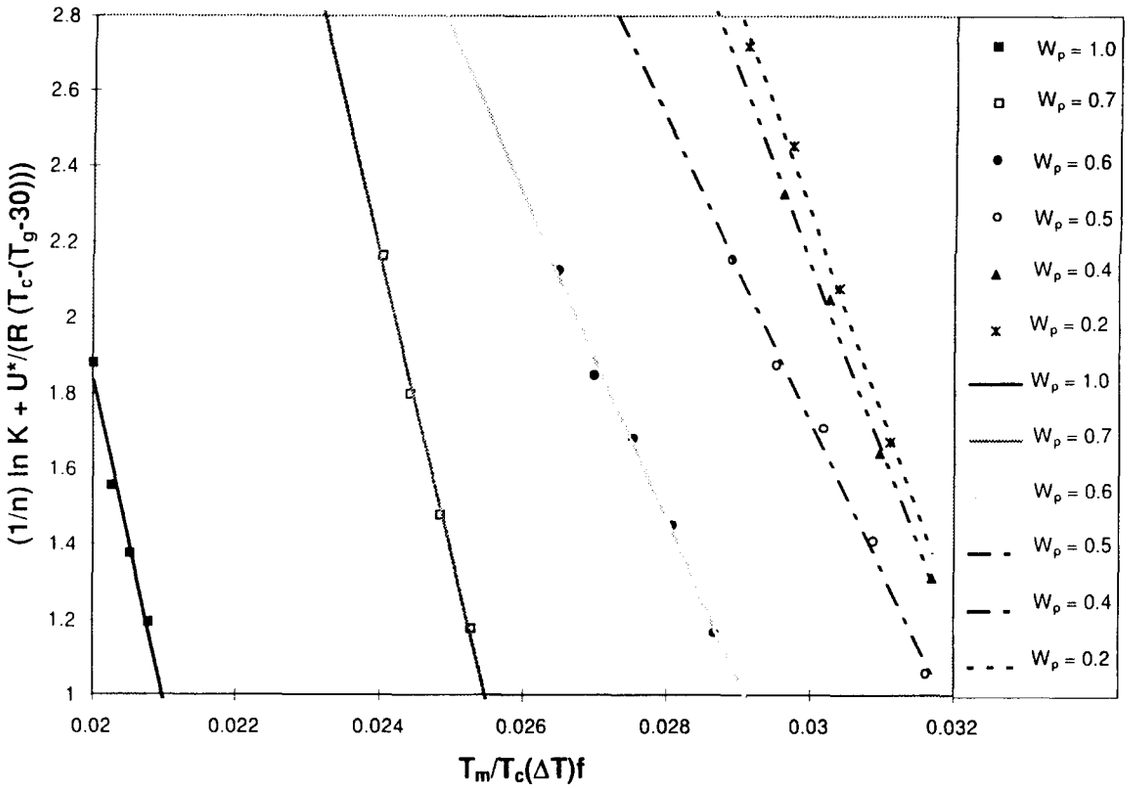

Figure 5 Hoffman–Lauritzen plot

Table 7 $(1/n)\ \ln K$ at $\Delta T = 39$K. D represents data; E represents estimated using equation (11)

W_p	$(1/n)\ \ln K$	K^n
1.0	− 10.754 (E)	2.13×10^{-5}
0.7	− 6.543 (E)	1.44×10^{-3}
0.5	− 2.256 (D)	1.05×10^{-1}
0.3	− 2.205 (D)	1.10×10^{-1}
0.2	− 2.117 (D)	1.20×10^{-1}

the pure iPP and two orders of magnitude greater than 70 wt%. This crystallization rate is constant for $W_p < 0.5$ within experimental error. The accelerated crystallization rate at lower W_p, for a given ΔT, coincides with the presence of excess diluent crystals. The mechanism of this acceleration cannot be isolated in this study since nucleation and growth have not been decoupled.

CONCLUSIONS

iPP crystallization kinetics were accurately described by the Avrami equation for $W_p = 0.20$–0.70 in the T_c range 390–396 K. For iPP concentrations less than 75 wt%, HMB crystallized prior to iPP crystallization onset. For iPP concentration greater than 75 wt-%, diluent crystallization was not detectable via material balance; however, SEM photomicrographs indicated that HMB resided at interspherulitic boundaries[2]. Therefore, polymer crystallization preceded diluent rejection and crystallization. This interpretation agrees with the phase diagram and proposed relative kinetics of phase transitions.

Increasing ΔT resulted in faster growth for all polymer concentrations. Using $(1/n)\ \ln K$ as a measure of crystallization rate, it was concluded that the rate at the same supercooling for polymer concentrations below the equilibrium eutectic ($W_p < 0.50$) did not vary significantly, indicating that increasing the amount of crystallized diluent did not influence the iPP crystallization time scale. However, iPP crystallization rate in the pure state is slower than in the presence of crystallized diluent at the same supercooling.

The crystallization of iPP in the presence of HMB fits the Hoffman–Lauritzen model in the T_c range 390–395K for $W_p = 0.20$–0.70, and $T_c = 398$–401K for $W_p = 1.00$. Since the model is based on secondary nucleation of chain-folding polymer molecules, it appears that the crystal growth mechanism is not measurably changed by the presence of HMB; that is, iPP grows by chain-folding of molecules from the melt blend independent of melt polymer concentration and the presence of crystallized HMB.

For a given thermodynamic driving force, samples below the equilibrium eutectic polymer concentration, $W_p < 0.50$, were estimated to grow at least two orders of magnitude faster than samples $W_p = 0.70$–1.00.

ACKNOWLEDGEMENTS

The authors gratefully acknowledge the continued generous financial support of the Central Research Technology Development Laboratory of the 3M Company St. Paul, MN and the Texas Advanced Technology Program.

REFERENCES

1. Alwattari, A. and Lloyd, D. R., *Journal of Membrane Science*, 1991, **64**, 55–68.
2. Alwattari, A. A. and Lloyd, D. R., *Polymer*, 1994, **35**, 2710–2715.
3. Flory, P. J., *Principles of Polymer Chemistry*. Cornell University Press, Ithaca, 1965, pp. 507–576.
4. Scott, R. L., *Journal of Chemical Physics*, 1949, **17**, 279–284.
5. Smith, P. and Manley-St.John, R., *Macromolecules*, 1979, **12**, 483–491.

6. Kim, S.S. and Lloyd, D.R., *Polymer*,, 1992, **33**, 1026–1057.
7. Tammann, G. D. *The States of Aggregation*. Van Nostrand, New York, 1925, Chapter 9.
8. Avrami, M., Journal of Chemical Physics, 1939, **7**, 1103–1112; 1940, **8**, 212–224; 1941, **9**, 177–184.
9. Vasanthakumari, R., *Polymer*, 1981, **22**, 862–865.
10. Martuscelli, E., Pracella, M., Avella, M., Greco, R. and Ragosta, G., *Polymer Blends—Processing, Morphology and Properties* Plenum, New York, 1980.
11. Hoffman, J. D., Davis, G. T. and Lauritzen, J. I., *Treatise on Solid State Chemistry*, ed. N. B. Hannay. Plenum, New York, 1976, Chapter 7.
12. Natta, G. and Corradini, P., *Il Nuovo Cimento (Supplemento)*, 1960, **15**, 9–51.
13. Lauritzen, J. I. and Hoffman, J. D., *Journal of Applied Physics*, 1973, **44**, 4340–4352.
14. Thomas, D. G. and Stavely, L. A. K., *Journal of the Chemical Society*, 1952, **4**, 4569–4577.
15. Wang, Y. F. and Lloyd, D. R., *Polymer*, 1993, **34**, 2324–2329.
16. Flory, P. J. and McIntyre, A. D., *Journal of Polymer Science*, 1955, **18**, 590–591.
17. Morgan, L. B., Lester, G. R., Keller, A., Hartley, F. D. and Lord, F. W., *Transactions of the Royal Society, London*, 1954, **A921**, 1–3.
18. Van Krevelen, D. W. and Hoftyzer, P. J., *Properties of Polymers*. Elsevier, Amsterdam, 1976.
19. Wunderlich, B., *Macromolecular Physics*, Vol. 3. Academic, New York, 1980.
20. Clark, E. J. and Hoffman, J. D., *Macromolecules*, 1984, **17**, 878–885.
21. Zwiers, R. J. M., Gogolewski, S. and Pennings, A. J., *Polymer*, 1983, **24**, 167–174.
22. Spaght, M. E., Benson, T. S. and Parks, G. S., *Journal of Physics and Chemistry*, 1932, **36**, 882–888.
23. Tseng, H. S., Ph.D. thesis 1985, University of Texas at Austin, TX, Appendix II.
24. Wittmann, J. C. and Manley-St.John, R., *Journal of Polymer Science: Polymer Physics Edition*, 1977, **15**, 1089–1100.
25. Hodge, A. M., Kiss, G., Lotz, B. and Wittmann, J. C., *Polymer*, 1982, **23**, 985–990.
26. Lauritzen, J. I. and Hoffman, J. D., *Journal of Research of the National Bureau of Standards*, 1960, **64A**, 73–102.
27. Hoffman, J. D., *Society of Plastics Engineering. Transactions*, 1964, **4**, 315–362.
28. Smith, P. and Pennings, A. J., *Polymer*, 1974, **15**, 413–419.
29. Wunderlich, B., *Macromolecular Physics*, Vol. 2. Academic, New York, 1976.
30. Tammann, G., *The States of Aggregation*, D. Van Nostrand Company, New York, 1925.
31. Tomka, J., *European Polymer Journal*, 1968, **4**, 237–240.
32. Grenier, D. and Prud'Homme, R. E., *Journal of Polymer Science: Polymer Physics Edition*, 1980, **18**, 1655–1657.
33. Monasse, B. and Haudin, J. M., *Colloid and Polymer Science*, 1986, **264**, 117–122.
34. Lim, G. B. A. and Lloyd, D. R., *Polymer Engineering Science*, 1993, **33**, 513–521.
35. Khoury, F. and Passaglia, E., *Treatise on Solid State Chemistry*, ed. N. B. Hannay. Plenum, New York, 1976, Chapter 6.
36. Stein, R. S. and Powers, J., *Journal of Polymer Science*, 1962, **56**, S9.
37. Escleine, J. M., Monasse, B., Wey, E. and Haudin, J. M., *Colliod and Polymer Science*, 1984, **262**, 366–372.
38. Smith, P. and Pennings, A. J., *Brritish Polymer Journal*, 1977, **9**, 258–263.
39. Wang, Y. F., Ph.D. thesis 1989, University of Texas at Austin, TX, Chapter 4.
40. Monasse, B. and Haudin, J. M., *Colloid and Polymer Science*, 1985, **263**, 822–831.
41. Burns, J. R. and Turnbull, D., *Journal of Applied Physics*, 1966, **37**, 4021–4026.
42. Turnbull, D. and Fisher, J. C., *Journal of Chemistry and Physics*, 1949, **17**, 71–74.
43. Kennedy, M. A., Turturro, G., Brown, G. R. and St-Pierre, L. E., *Journal of Polymer Science: Polymer Physics Edition*, 1983, **21**, 1403–1413.
44. Wang, Y. F., Ph.D. thesis 1989, University of Texas at Austin, TX, Appendix to Chapter 3.